Extended Abstract: Flight & Ground Testing Data Set for an Unmanned Aircraft: Great Planes Avistar Elite

Or D. Dantsker *
Al Volo LLC, Urbana, IL 61801

Renato Mancuso†
Boston University, Boston, MA 02215

In the past several years, there has been a major increase in the popularity of unmanned aerial vehicles (UAVs) for research, military, commercial, and civilian applications. Part of this uptrend in UAV use includes increase in the research related to them. There have been UAVs used to study aerodynamic qualities,[1,2] especially in high angle-of-attack conditions.[3–5] Others have been used as testbeds to develop new control algorithms.[6–11] Additionally, some unmanned aircraft are used as low-cost stand-ins for experiments that are too risky or costly to perform on their full scale counterparts.[12–15] Yet other times, unmanned aircraft are developed to explore new aircraft configurations[16–19] or flight hardware.[20–22]

Development of a UAV platform takes several stages. First the airframe must be developed, which may involve design creation and construction, in the case with a custom design, or just construction, in the case of an already designed and pre-constructed commercial-off-the-shelf airframe (often a model aircraft kit). Next, instrumentation will follow a similar development route, depending on whether it is custom or commercial-off-the-shelf. Then comes ground testing, which may involve loads testing, moment of inertia measurement, and pre-flight combined systems testing. In summation, these stages become extremely costly in terms of resources as well as time. A research group may spend many months or possibly years to develop an aircraft, which may only be flight tested for a limited time.

This paper will present a data set for a trainer-type unmanned aircraft, a Great Planes Avistar Elite, which can be seen in Figure 1. This will be the second of a series of aircraft that will be published online and freely available as part of the upcoming Subscale Flight and Ground Testing (SFGT) Database[a].[23] In addition to flight testing data, photos and video of the flight tests from both on-board and on-ground will we published. Data from ground measurement and testing, including 3D scanning, computational tools, propeller performance testing, and moment of inertia testing, will be presented in this paper as well as published on the SFGT Database. Data reduction techniques used for the above testing will also be presented in this paper. Additional details regarding construction and instrumentation is also provided in this paper.

Aircraft Development and Specifications

The Great Planes Avistar Elite is a commercially available model aircraft that has been often used in research.[24–28] The airframe was constructed mainly following manufacturer recommendation with the exception of the propulsion system change and some small improvements to the control surface actuator linkages. The aircraft was originally designed intended to use an internal combustion gasoline engine, however, the aircraft was adapted to use an electric propulsion system as it provides near constant performance, increased reliability, and low vibrations. Aircraft construction photos can be found in Figure 2 and specifications can be found in Tables 1 and 2.

The aircraft was instrumented with an Al Volo FDAQ[29] data acquisition system. The system operates at 400 Hz and integrates with a 9 degree-of-freedom (9-DOF) XSens MTi-G-700[30] IMU with a GPS receiver. A pitot-static probe

*Aero-Mechanical Engineer. ordantsker@alvolo.us
†Assistant Professor, Department of Computer Science. rmancuso@bu.edu
[a]The SFGT Database will be made public before the time of publication and will include other aircraft such as a 26%-scale Cub Crafters CC11-100 Sport Cub S2[23] and 22% scale Cessna 182 Skylane.

will be installed half-way down the span of the left wing in the near future. The pilot commands are also recorded by measuring the pulse width modulation (PWM) signals generated by receiver. The propulsion system information is logged by FDAQ through an interfaces with the Castle Creations ESC. Using the sensors, the system is able to log and transmit: 3D linear and angular accelerations, velocities, and position along with GPS location; pitot-static probe airspeed; 3D magnetic field strength and heading; control surface deflections; and motor voltage, current, RPM, and power. Specifications for the instrumentation can be found in Table 3.

Figure 1. The flight-ready instrumented Great Planes Avistar Elite.

Table 1. Airframe physical specifications.

Geometric Properties	
Overall Length	55.0 in (1395 mm)
Wing Span	62.5 in (1590 mm)
Wing Area	672 in^2 (43.3 dm^2)
Aspect Ratio	6.62
Inertial Properties	
Weight	
Empty (w/o Battery)	7.53 lb (3.415 kg)
4S LiPo Battery	1.17 lb (0.530 kg)
Gross Weight	8.70 lb (3.945 kg)
Wing Loading	29.8 oz/ft^2 (90.9 gr/dm^2)

Table 2. Airframe component specifications.

Construction	Built-up balsa and plywood structure, aluminum wing tube, aluminum landing gear, abs canopy, and plastic film sheeted.
Flight Controls	
Controls	Aileron (2), elevator, rudder, throttle, and flaps (2)
Transmitter	Futaba T14MZ
Receiver	Futaba R6014HS
Servos	(6) Futaba S3004
Regulator Distribution	Castle Creations CC BEC
Receiver Battery	Thunder ProLite 20c 2S 7.4V 450 mAh
Propulsion	
Motor	AXI 4120/14 Outrunner
ESC	Castle Creation Phoenix ICE 75 Amp Brushless Speed Controller
Propeller	APC 13x8E
Motor Flight Pack	Thunder Power ProPower 30c 4S 14.8 V 5 Ah lithium polymer battery
Flight Time	10-20 min

Table 3. Instrumentation specifications.

Data acquisition system	Al Volo FDAQ 400 Hz system
Sensors	
Inertial measurement unit	XSens MTi-G-700 AHRS with GPS
Airspeed sensor	Al Volo Pitot Static Airspeed Sensor
Motor sensor	Al Volo Castle ESC Interface
Power	
Regulator	Built into FC+DAQ
Battery	Thunder Power ProLiteX 3S 1350 mAh

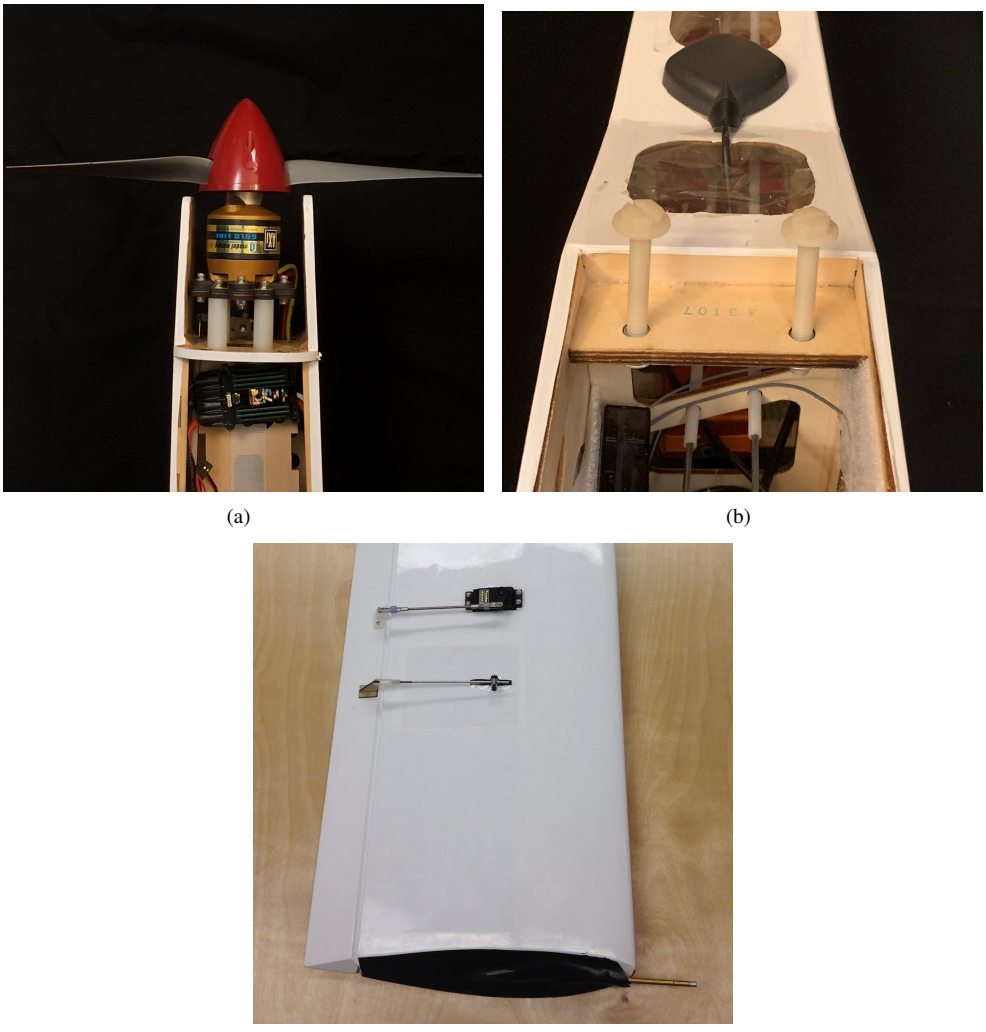

(a) (b)

(c)

Figure 2. Aircraft construction details: (a) nose of aircraft with brushless motor, propeller, and electronic speed controller (ESC), (b) rear of fuselage behind wing mounting location containing the inertial measurement unit (IMU) mounted inside and the GPS antenna ontop, and (c) outer wing with aileron servo and pitot probe.

Present Ground Measurement and Testing

To date, the Great Planes Avistar Elite aircraft has been extensively measured and tested. This includes 3D scanning of the entire aircraft[31] and testing the 3D model generated in several computational tools.[32]

3D Scanning

The 3D scanning was performed using a ZCorporation ZScanner 800 self-positioning handheld 3D scanner.[33] The 3D point cloud output from the scanner was processed using a previously written MATLAB script called AirplaneScan. The 3D scan pointcloud of the Avistar UAV was translated and rotated from its original skewed angle and location. The tip of the nosecone was placed at the origin with the x-axis toward the left, the y-axis out the tail, and the z-axis up; it should be noted that a non-standard coordinate system is used. The points on the right half of the airplane were discarded, and then the points on the left half were mirrored to the right with the exception of the nose gear, which was not mirrored.The resulting processed 3D point cloud can be seen in a 3-view and an isometric view in Fig. 3. The processed point cloud was then sliced multiple times to yield the cross sections of the fuselage, wings, and tail sections; the points were plotted in Figs. 4-7.

The pointcloud slices generated by the AirplaneScan MATLAB script provided dimensions and coordinates for all of the flight surfaces. It is important to note that the wing has a constant airfoil throughout the span and the horizontal and vertical stabilizers each have continuously varying airfoils from root to tip. The coordinates of each airfoil produced are plotted in Fig. 8. The wing airfoil coordinates were previously verified[31] with coordinates for the AVISTAR airfoil found on the UIUC Airfoil Database[34] and the stabilizer airfoils were verified with manual measurements. The dimensions of each flight surface and the airfoil locations are given in Table 4; the coordinate system used has the x-axis towards the tail, the y-axis towards the right wing, and the z-axis up. Using the fuselage geometry from the 3D scan and the aforementioned flight surface geometry, a computer aided design (CAD) model of the aircraft was made in SolidWorks (see Fig. 9).

Table 4. Avistar UAV flight surface specifications.

Wing							
LE x pos	**LE z pos**	**Incidence**	**y span pos**	**Chord**	**Offset**	**Dihedral**	**Airfoil**
380.4 mm	95.5 mm	3.58 deg	0 mm	237.10 mm	0 mm	0.9 deg	AVISTAR
-	-	-	793.75 mm	237.10 mm	0 mm	-	AVISTAR
Horizontal Stabilizer							
LE x pos	**LE z pos**	**Incidence**	**y span pos**	**Chord**	**Offset**	**Dihedral**	**Airfoil**
1160 mm	-2.04 mm	2.36 deg	0 mm	210 mm	0 mm	0 deg	AVISTARHSTABROOT
-	-	-	291 mm	110 mm	100 mm	-	AVISTARHSTABTIP
Vertical Stabilizer							
LE x pos	**LE z pos**	**Incidence**	**y span pos**	**Chord**	**Offset**	**Dihedral**	**Airfoil**
1160 mm	17.96 mm	2.36 deg	0 mm	273 mm	-95 mm	0 deg	AVISTARVSTABROOT
-	-	-	200 mm	96 mm	133 mm	-	AVISTARVSTABTIP

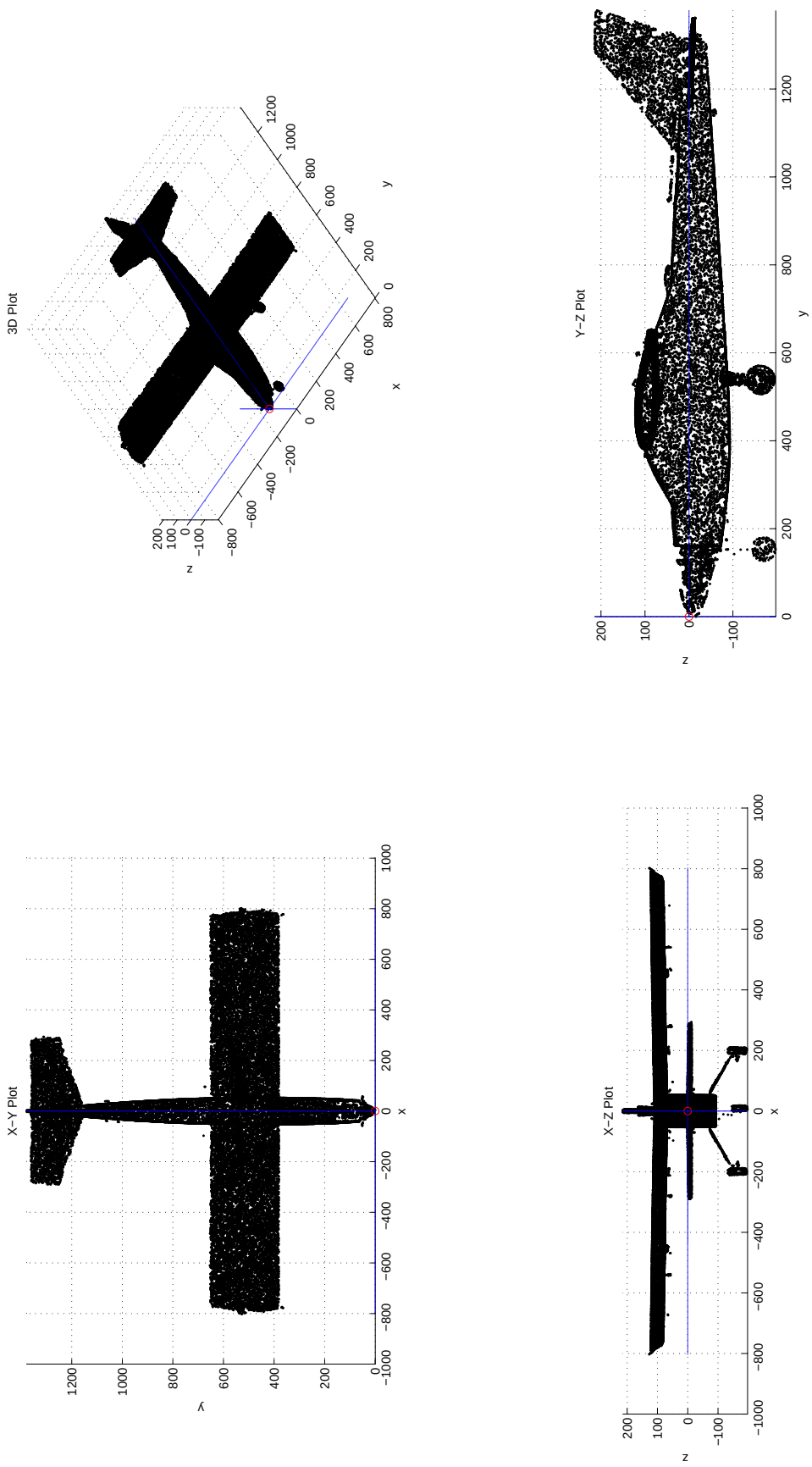

Figure 3. 3-view and isometric plots of the Avistar Elite scan after processing.

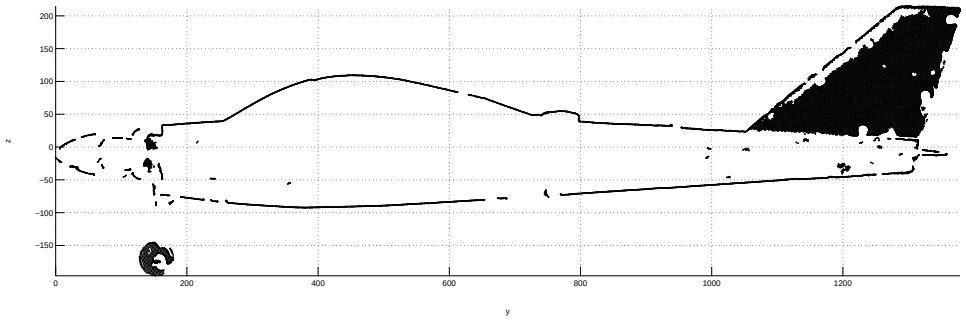

Figure 4. Plot of Y-Z slice of the 3D scan point cloud between x=-5 and x=5.

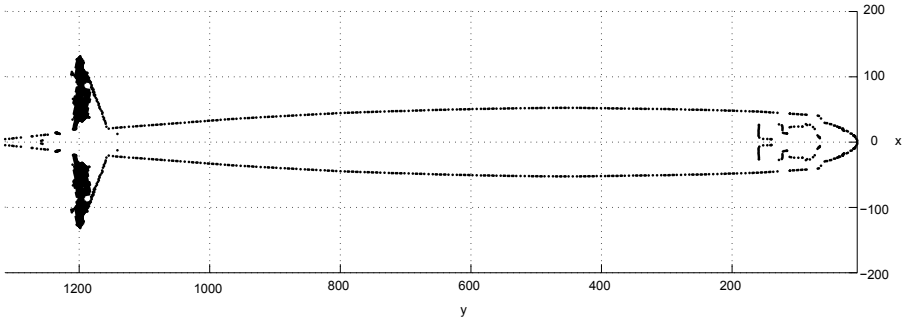

Figure 5. Plot of X-Y slice of the 3D scan point cloud between z=0 and z=1.

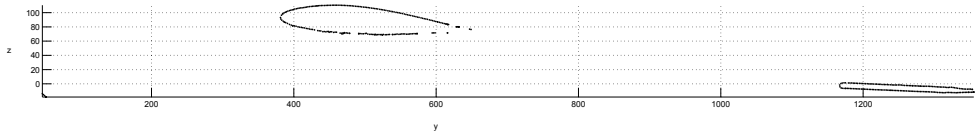

Figure 6. Plot of Y-Z slice of the 3D scan point cloud between x=53 and x=55.

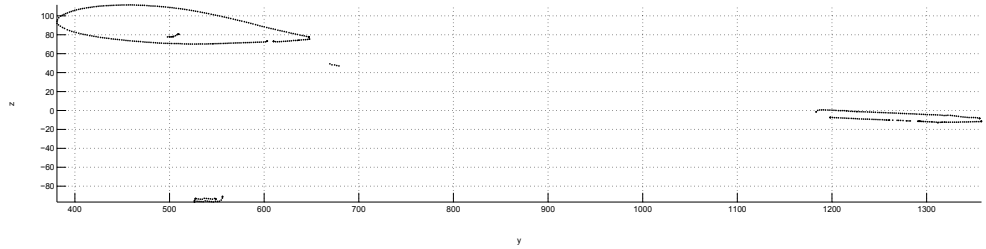

Figure 7. Plot of Y-Z slice of the 3D scan point cloud between x=98 and x=100.

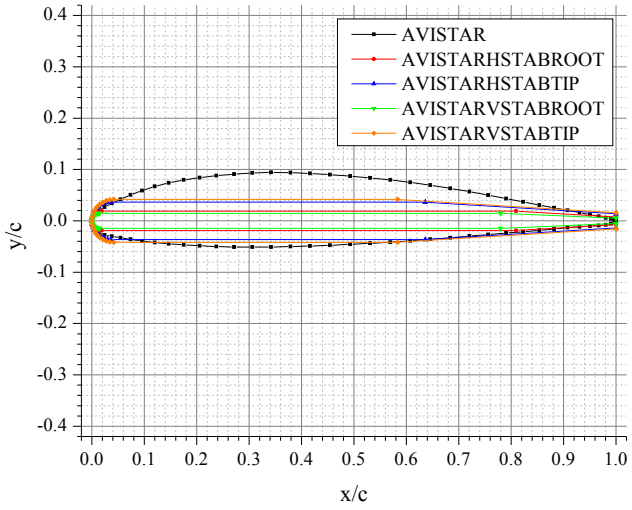

Figure 8. The airfoils used on the Avistar Elite.

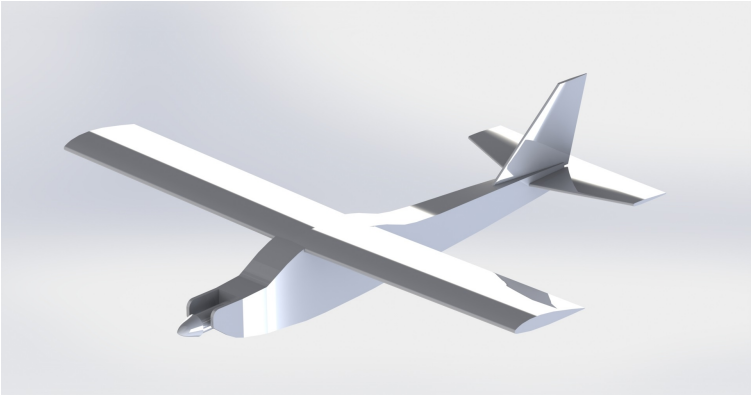

Figure 9. A SolidWorks CAD model of the Avistar Elite.

Computational Tool

The 3D model of the Great Planes Avistar Elite was input into 3 types of computational tools. Two low-order computational tools based on lifting-line theory, XFLR5[35] and Athena Vortex Lattice (AVL),[36] as well as one high-order method, using the computational fluid dynamics tool Ansys Fluent, were used.

The airfoil coordinates and flight surface location generated by the 3D scan were entered into XFLR5, and the resultant model can be seen in Fig. 10. The fuselage was withheld from the aerodynamics model per recommendations provided in the documentation of XFLR5, as mentioned earlier. In order to test the aerodynamics model in XFLR5, each of the airfoils needed to be run for all possible Reynolds numbers and angles-of-attack. The Reynolds number was swept between 10,000 and 500,000 and the angle-of-attack was swept between -15 deg and 15 deg, to provide the greatest possible operating range for both the wing and stabilizers. XFLR5 was used to run the Avistar aerodynamics model for a flight speed of 14 m/s (46 mph) in inviscid mode.

Similarly, the aircraft geometry was implemented into the aerodynamics analysis tool, AVL. The fuselage geometry was created using the 3D scan point cloud. The area of each fuselage section along the length was calculated and a circular cross section of equivalent area was implemented into AVL for the analysis. The same flight speeds mentioned above were used for the analysis. The analyzed geometry is given in Fig. 11. AVL is an inviscid analysis, meaning that viscous effects are not taken into account for the aerodynamic analysis of the Avistar. Though viscous effects are not taken into account, the fuselage can be included in the analysis, allowing the user to calculate how it can effect the stability derivatives.

Finally, a CFD simulation was performed using Ansys Fluent.[37] Using the CAD model described earlier, a mesh was created using the Fluent meshing tool with 4 million cells, as shown in Fig. 12. The CFD simulation used a with K-epsilon (k-ε) turbulence model and was run on an 18-core Intel Xeon Processor E5-2697 v4 workstation with 32 GB DDR4 and a 4 GB GDDR5 NVIDIA Quadro K4200, which has 1344-CUDA cores. The freestream velocity of the analysis was 14 m/s, which operated under standard atmospheric conditions. The analysis was conducted for angles-of-attack from -4 to 14 deg, with increments of 2 deg. Ansys Fluent predicted that aircraft stalls at approximately 10 to 12 deg and thus the stability derivatives were calculated using data from -4 to 8 deg, which appeared linear.

Streamlines for the wing, tail, and fuselage from the CFD analysis are shown in Figs. 13, 14, and 15, respectively. Warmer colors in the streamline figure indicate higher speeds while cooler colors show lower speeds. As seen, the flow is fully attached on the wing. At 4 deg, warmer shades of streamlines indicate higher flow acceleration compared to 10 and 14 deg. Beyond stall at 14 deg, flow separation was observed near the root while the flow is attached near the tip. This shows that the onset of stall begins near the hub region instead of the tip. Flow streamlines are attached on the tail until 10 deg but large separation can be observed for 14 deg. There is also a significant spanwise flow near the root of the horizontal tail at 14 deg. This is due the interference from the flow from the fuselage as shown below. Similarly, at lower angles-of-attack (4 deg), the flowfield is primarily two-dimensional on the fuselage. However, at higher angles-of-attack (14 deg) the flow becomes highly three-dimensional due to flow separation from the fuselage.

The results from each of the analysis are tabulated in Table 5 along with data from a flight test. The low order tools and CFD results predicted lift curve slope and zero angle-of-attack values within the same order of magnitude of the flight test and had similar trends. Ansys had the closest lift curve slope to the flight test, which may be attributed to 3D effects not accounted for in the low order tools, as XFLR5 and AVL had similar predictions. The drag predictions from AVL were lower than those from experimental data, XFLR5 and Ansys, which was attributed to how AVL does not include viscous effects. The drag predicted from Ansys Fluent is the closest to the to flight test data results although the drag curve slope for XFLR5 and Ansys Fluent were lower than the experimental results by an order of magnitude.

Table 5. Aircraft characteristics and stability derivatives for each analysis run

	XFLR5	AVL	Ansys Fluent	Flight Test
$C_{L\alpha}$	0.0827	0.0810	0.0667	0.0606
$C_{D\alpha}$	0.0075	0.0043	0.0067	0.0237
$C_{M\alpha}$	-0.0249	-0.0193	-0.0340	–
C_{Lo}	0.357466	0.33088	0.3875	0.5345
C_{Do}	0.020282	0.00633	0.05512	0.0489
C_{Mo}	-0.00799	-0.06364	-0.00659	–

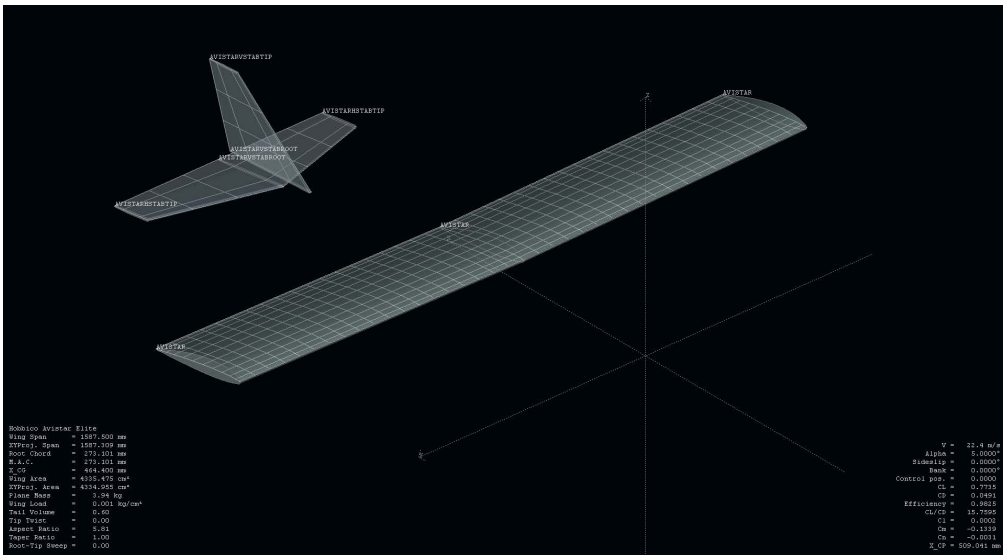

Figure 10. XFLR5 aerodynamics model for the Avistar UAV.

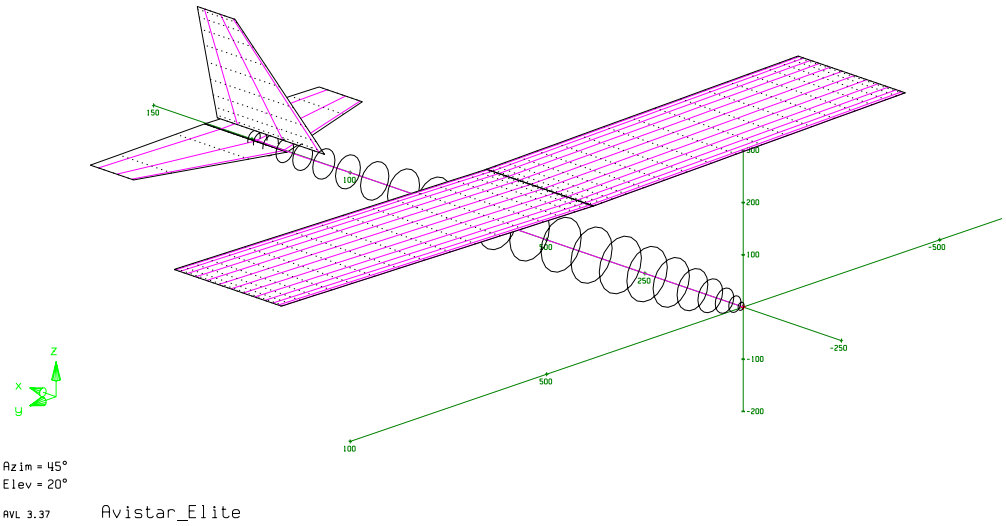

Figure 11. AVL aerodynamics model for the Avistar UAV.

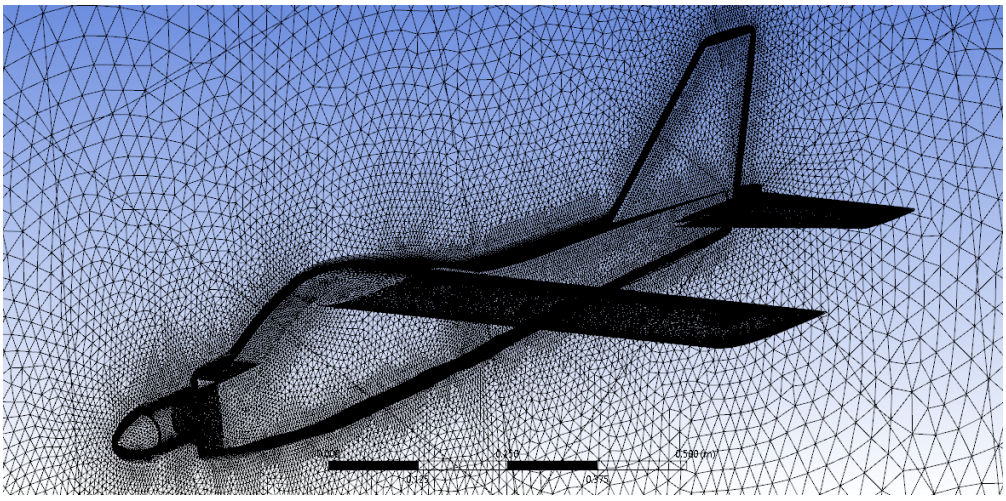

Figure 12. Avistar UAV CAD model meshed in Ansys Fluent with 4 million cells.

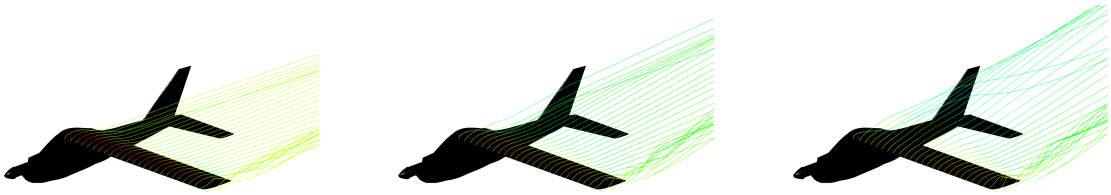

(a) (b) (c)

Figure 13. Wing streamlines from Ansys Fluent at angles-of-attack of: (a) 4 deg, (b) 10 deg, and (c) 14 deg.

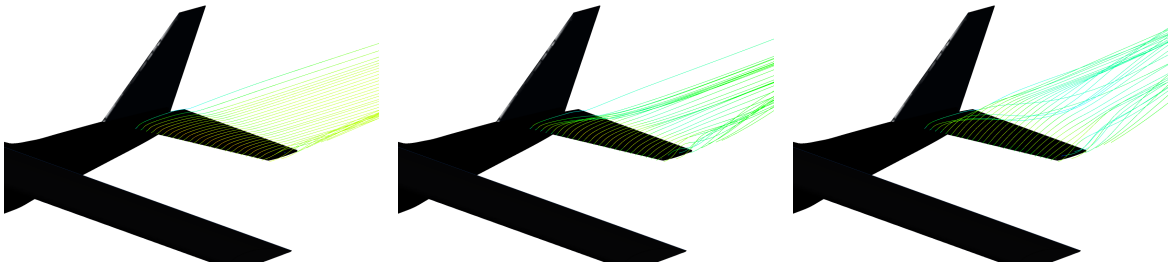

(a) (b) (c)

Figure 14. Tail streamlines from Ansys Fluent at angles-of-attack of: (a) 4 deg, (b) 10 deg, and (c) 14 deg.

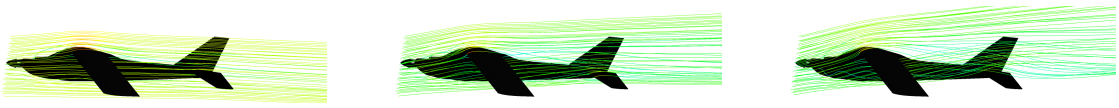

(a) (b) (c)

Figure 15. Fuselage streamlines from Ansys Fluent at angles-of-attack of: (a) 4 deg, (b) 10 deg, and (c) 14 deg.

Planned Ground and Flight Testing

Ground and flight testing is planned for the winter and spring of 2019. Ground testing will include moment of inertia testing of the aircraft using a testing apparatus at the University of Illinois at Urbana-Champaign[27] as well as complete parametrization of the flight control surfaces to the commanded servo signals (PWM) and control deflections. Performance testing of the aircraft propeller is also planned using a mobile measurement rig.[38] Flight testing planned will include a range of maneuvers outlined in Table 6.

Table 6. Flight Test Maneuvers Planned

Maneuver	Flap Configuration	Description
Idle Descent	Clean	Descent using idle power with different amounts of trim
Phugoid	Clean	Entry with aircraft trimmed and elevator deflected to change airspeed;
Roll Response	Clean	Aileron momentarily deflected to 20 deg with roll rate of at least 30 deg of roll
Rudder Response	Clean	Rudder momentarily deflected to 25 deg
Power-Off Stall		Entry with wings level;
	Clean	limited elevator deflection
		full elevator deflection
	Half-Flaps	limited elevator deflection
		full elevator deflection
	Full-Flaps	limited elevator deflection
		full elevator deflection
Power-Off Spin		Entry with wings level;
	Clean	limited elevator deflection
		full elevator deflection
	Half-Flaps	limited elevator deflection
		full elevator deflection
	Full-Flaps	limited elevator deflection
		full elevator deflection
Takeoff	Clean	Trimmed with either no of limited no elevator deflection;
	Half-Flaps	
	Full-Flaps	
Landing	Clean	Trimmed;
	Half-Flaps	
	Full-Flaps	

References

[1]Lykins, R. and Keshmiri, S., "Modal Analysis of 1/3-Scale Yak-54 Aircraft Through Simulation and Flight Testing," AIAA Paper 2011-6443, AIAA Atmospheric Flight Mechanics Conference, Portland, Oregon, Aug. 2011.

[2]Johnson, B. and Lind, R., "Characterizing Wing Rock with Variations in Size and Configuration of Vertical Tail," *Journal of Aircraft*, Vol. 47, No. 2, 2010, pp. 567–576.

[3]Perry, J., Mohamed, A., Johnson, B., and Lind, R., "Estimating Angle of Attack and Sideslip Under High Dynamics on Small UAVs," Proceedings of the ION-GNSS Conference, Savannah, Georgia, 2008.

[4]Uhlig, D., Sareen, A., Sukumar, P., Rao, A. H., and Selig, M. S., "Determining Aerodynamic Characteristics of a Micro Air Vehicle Using Motion Tracking," AIAA Paper 2010-8416, AIAA Guidance, Navigation, and Control Conference, Toronto, Ontario, Canada, Aug. 2010.

[5]Dantsker, O. D. and Selig, M. S., "High Angle of Attack Flight of a Subscale Aerobatic Aircraft," AIAA Paper 2015-2568, AIAA Applied Aerodynamics Conference, Dallas, Texas, Jun. 2015.

[6]Mockli, M., *Guidance and Control for Aerobatic Maneuvers of an Unmanned Airplane*, Ph.D. thesis, ETH Zurich, Department of Mechanical and Process Engineering, 2006.

[7]Frank, A., McGrewy, J. S., Valentiz, M., Levinex, D., and How, J. P., "Hover, Transition, and Level Flight Control Design for a Single-Propeller Indoor Airplane," AIAA Paper 2007-6318, AIAA Guidance, Navigation, and Control Conference, Hilton Head, South Carolina, Aug. 2007.

[8]Johnson, E. N., Wu, A. D., Neidhoefer, J. C., Kannan, S. K., and Turbe, M. A., "Test Results of Autonomous Airplane Transitions Between Steady-Level and Hovering Flight," *Journal of Guidance, Control, and Dynamics*, Vol. 31, No. 2, 2008, pp. 358–370.

[9]Gaum, D. R., *Aggressive Flight Control Techniques for a Fixed-Wing Unmanned Aerial Vehicle*, Master's thesis, Stellenbosch University, Department of Electrical and Electronic Engineering, 2009.

[10]Bilodeau, P. R., Poulin, E., Gagnon, E., Wong, F., and Desbiens, A., "Control of a Hovering Mini Fixed Wing Aerial Vehicle," AIAA Paper 2009-5794, AIAA Guidance, Navigation and Control Conference, Chicago, Illinois, Aug. 2009.

[11]Johnson, B. and Lind, R., "Trajectory Planning for Sensing Effectiveness with High Angle-of-Attack Flight Capability," AIAA Paper 2012-0276, AIAA Aerospace Sciences Meeting, Nashville, Tennessee, Jan. 2012.

[12]Jordan, T. L. and Bailey, R. M., "NASA Langley's AirSTAR Testbed: A Subscale Flight Test Capability for Flight Dynamics and Control System Experiments," AIAA Paper 2008-6660, AIAA Atmospheric Flight Mechanics Conference, Honolulu, HI, Aug. 2008.

[13]Ragheb, A. M., Dantsker, O. D., and Selig, M. S., "Stall/Spin Flight Testing with a Subscale Aerobatic Aircraft," AIAA Paper 2013-2806, AIAA Applied Aerodynamics Conference, San Diego, CA, Jun. 2013.

[14]Bunge, R. A., Savino, F. M., and Kroo, I. M., "Approaches to Automatic Stall/Spin Detection Based on Small-Scale UAV Flight Testing," AIAA Paper 2015-2235, AIAA Atmospheric Flight Mechanics Conference, Dallas, Texas, Jun. 2015.

[15]Dantsker, O. D., Ananda, G. K., and Selig, M. S., "GA-USTAR Phase 1: Development and Flight Testing of the Baseline Upset and Stall Research Aircraft," AIAA Paper 2017-4078, AIAA Applied Aerodynamics Conference, Denver, Colorado, June 2017.

[16]Risch, T., Cosentino, G., Regan, C., Kisska, M., and Princen, N., "X-48B Flight-Test Progress Overview," AIAA Paper 2009-934, AIAA Aerospace Sciences Meeting, Orlando, FL, Jan. 2009.

[17]Lundstrom, D. and Amadori, K., "Raven: A Subscale Radio Controlled Business Jet Demonstrator," International Congress on the Aeronautical Sciences Systems (ICUAS), Anchorage, Alaska, Sep. 2008.

[18]Regan, C. D. and Taylor, B. R., "mAEWing1: Design, Build, Test - Invited," AIAA Paper 2016-1747, AIAA Atmospheric Flight Mechanics Conference, San Diego, California, Jun. 2016.

[19]Regan, C. D., "mAEWing2: Conceptual Design and System Test," AIAA Paper 2017-1391, AIAA Atmospheric Flight Mechanics Conference, Grapevine, Texas, Jun. 2017.

[20]Leong, H. I., Keshmiri, S., and Jager, R., "Evaluation of a COTS Autopilot and Avionics System for UAVs," AIAA Paper 2009-1963, AIAA Infotech@Aerospace, Seattle, Washington, April. 2009.

[21]Esposito, J. F. and Keshmiri, S., "Rapid Hardware Interfacing and Software Development for Embedded Devices Using Simulink," AIAA Paper 2010-3415, AIAA Infotech@Aerospace, Atlanta, Georgia, June 2010.

[22]Garcia, G. and Keshmiri, S., "Integrated Kalman Filter for a Flight Control System with Redundant Measurements," AIAA Paper 2012-2499, AIAA Infotech@Aerospace, Garden Grove, California, June 2012.

[23]Dantsker, O. D. and Mancuso, R., "Flight & Ground Testing Data Set for Subscale GA Aircraft: 26%-scale Cub Crafters CC11-100 Sport Cub S2," Accepted to the AIAA SciTech Forum, Jan. 2019.

[24]Mancuso, R., Dantsker, O. D., Caccamo, M., and Selig, M. S., "A Low-Power Architecture for High Frequency Sensor Acquisition in Many-DOF UAVs," Submitted to International Conference on Cyber-Physical Systems, Berlin, Germany, April 2014.

[25]Dantsker, O. D., Mancuso, R., Selig, M. S., and Caccamo, M., "High-Frequency Sensor Data Acquisition System (SDAC) for Flight Control and Aerodynamic Data Collection Research on Small to Mid-Sized UAVs," AIAA Paper 2014-2565, AIAA Applied Aerodynamics Conference, Atlanta, Georgia, June 2014.

[26]Dantsker, O. D., Loius, A. V., Mancuso, R., Caccamo, M., and Selig, M. S., "SDAC-UAS: A Sensor Data Acquisition Unmanned Aerial System for Flight Control and Aerodynamic Data Collection," *AIAA Infotech@Aerospace Conference, Kissimee, Florida, Jan 2015.*.

[27]Dantsker, O. D., Vahora, M., Imtiaz, S., and Caccamo, M., "High Fidelity Moment of Inertia Testing of Unmanned Aircraft," AIAA Paper 2018-4219, AIAA Applied Aerodynamics Conference, Atlanta, Georgia, Jun. 2018.

[28]Dantsker, O. D., Theile, M., and Caccamo, M., "A High-Fidelity, Low-Order Propulsion Power Model for Fixed-Wing Electric Unmanned Aircraft," AIAA/IEEE Electric Aircraft Technologies Symposium, Jul. 2018.

[29]Al Volo LLC, "Al Volo: Flight Data Acquisition Systems," http://www.alvolo.us.

[30]Xsens Technologies B.V., "XSens, MTi-G-700," https://www.xsens.com/products/mti-g-700/, Accessed Jan. 2016.

[31]Dantsker, O. D., "Determining Aerodynamic Characteristics of an Unmanned Aerial Vehicle using a 3D Scanning Technique," AIAA Paper 2015-0026, AIAA Aerospace Sciences Meeting, Kissimmee, Florida, Jan. 2015.

[32]Dantsker, O. D. and Vahora, M., "Comparison of Aerodynamic Characterization Methods for Design of Unmanned Aerial Vehicles," AIAA Paper 2018-0272, AIAA Aerospace Sciences Meeting, Kissimmee, Florida, Jan. 2018.

[33]ZCorporation, "The New ZScanner 800," www.zcorp.com/documents/182_ZScanner800-tearsheet-v05wb.pdf, Accessed Mar. 2013.

[34]UIUC Applied Aerodynamics Group, "UIUC Airfoil Coordinates Database," http://aerospace.illinois.edu/m-selig/ads/coord_database.html.

[35]Andre Deperrois, "XFLR5," http://www.xflr5.com/, Accessed Jun. 2017.

[36]Mark Drela, "AVL," http://web.mit.edu/drela/Public/web/avl/, Accessed Jun. 2017.

[37]ANSYS, Inc, "ANSYS Fluent: CFD Simulation," http://www.ansys.com/Products/Fluids/ANSYS-Fluent, Accessed Jun. 2017.

[38]Dantsker, O. D., Imtiaz, S., and Caccamo, M., "Propulsion System Testing and Optimization for a Long-Endurance Solar-Powered Unmanned Aircraft," Submitted to 2019 AIAA Applied Aerodynamics Conference, Dallas, Texas, June 2019.